Section 7

Global and regional climate models, sensitivity and impact experiments, response to external forcing

Soil subsidence in the 21st century simulated using anthropogenic climate change scenarios

M.M. Arzhanov
A.M. Obukhov Institute of Atmospheric Physics RAS, 3 Pyzhevsky, 119017 Moscow, Russia
arzhanov@ifaran.ru

Projected warming is most pronounced in the northern high latitudes. The surface temperature increase can result in changes in the thermal and hydrological conditions of permafrost [1]. Permafrost degradation and associated soil subsidence are assessed in simulations with a soil model developed at A.M. Obukhov Institute of Atmospheric Physics RAS [2-4]. This model is forced by monthly mean atmospheric fields simulated by the ECHAM5/MPI-OM coupled general circulation model using anthropogenic scenarios SRES A1B and A2.

Total extent of simulated near-surface permafrost in the Northern Hemisphere in 2001-2010 is about 16.7±2.3 million km^2. This area shrinks to 11.2±1.1 (7.9±0.8) million km^2 to the end of the 21st century under SRES A1B (A2) scenario. A similar value (7 million km^2) has been obtained for MIROC 3.2 model [5]. An even smaller permafrost area (about 1-4 million km^2) for the end of the 21st century is simulated by the CCSM3 model [6]. In the late 21st century, near-surface permafrost is expected to remain in central and eastern Siberia and in the high latitudes of northern America. In these regions, the active layer depth exceeds 1.5 m (2.0 m) under SRES A1B (A2) scenario. Subsurface permafrost turns to a relic form since 2050 (2030) in the regions near contemporary permafrost southern boundary in the Northern Hemisphere (Fig. 1). The model simulates substantial permafrost degradation in western Siberia and Alaska. Permafrost degradation is accompanied by a formation of taliks which penetrate to the depth of several meters within a few decades [7].

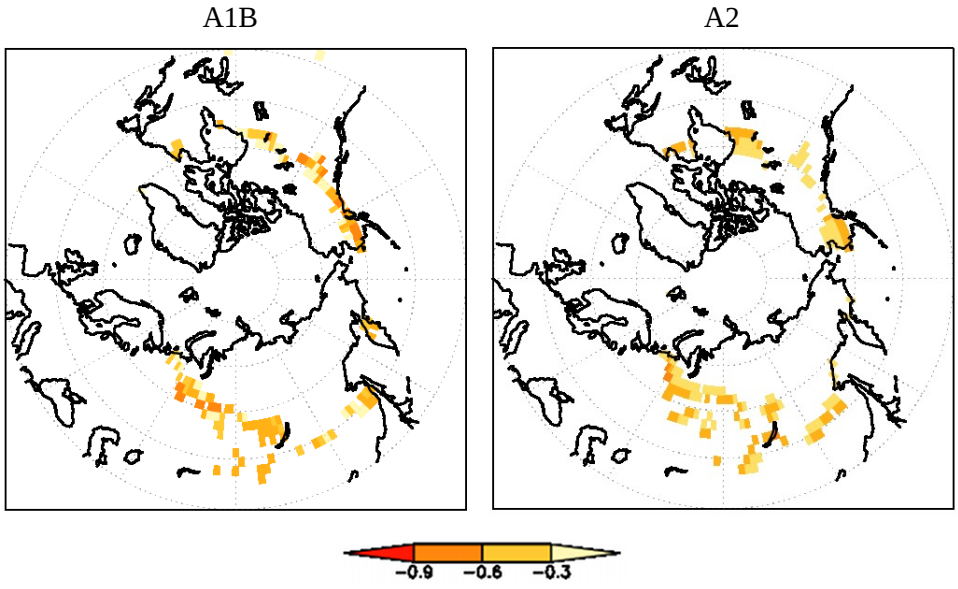

Fig. 1. Simulated thaw subsidence (meters) due to the subsurface permafrost degradation when applying SRES A1B and A2 scenarios in 2046-2055.

Most marked near-surface permafrost degradation is simulated for the last decades of the 21st century (Fig. 2). Permafrost thaw leads to cavities in soil pores, and the soil subsidence due to gravity. This soil subsidence is estimated based on [8].

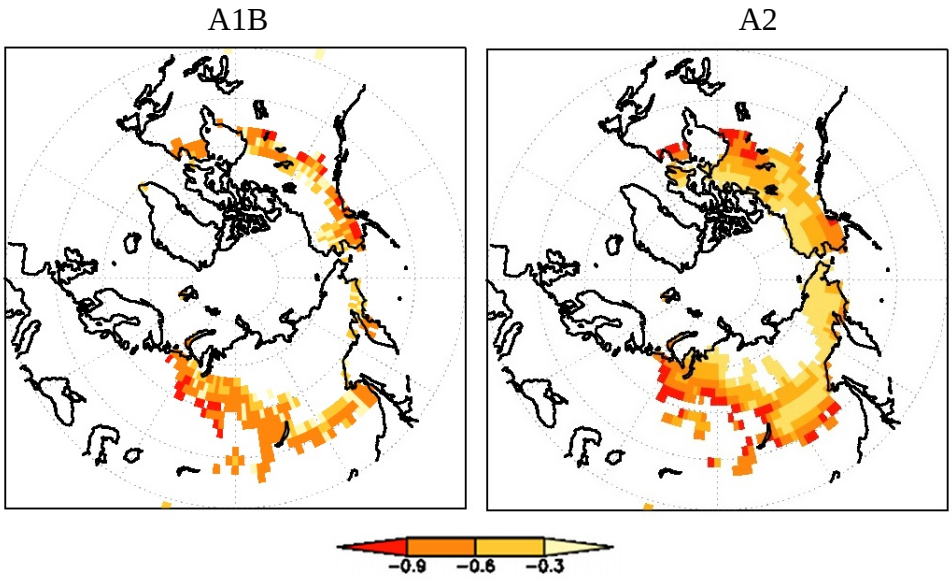

Fig. 2. Simulated thaw subsidence (meters) due to the subsurface permafrost degradation when applying SRES A1B and A2 scenarios in 2091-2100.

During the second half of the 21st century, simulated near-surface permafrost area with subsidence enlarges rapidly. Typical values of vertical shifts of soil layers amount to several tens of centimeters and reach up to 1.2 m locally (Fig. 2).

Acknowledgments
NATO Collaborative Linkage Grant 983 725, Grant of the RF President Nsh-5467.2012.5, The Russian Fondation for Basic Research, The program of the Earth Sciences Department of the Russian Academy of Sciences, Programs of the Russian Ministry for Science and Education (contracts 403 14.740.11.1043, 21.519.11.5004, and 11.519.11.5006), Russian Academy of Science 74-OK/11-4.

References

[1] Climate Change 2007: The Physical Science Basis. S. Solomon, D. Qin, I.M. Manning et al. (eds.). Cambridge: Cambridge University Press. 2007. 996 pp.
[2] Arzhanov, M. M., Eliseev, A. V., Demchenko, P. F., Mokhov, I. I., and V. Ch. Khon, 2008. Simulation of thermal and hydrological regimes of siberian river watersheds under permafrost conditions from reanalysis data. Izvestiya, Atmos. Ocean. Phys. 44 (1), 83–89.
[3] Arzhanov, M., Demchenko, P., Eliseev, A., Mokhov, I., 2008. Simulation of characteristics of thermal and hydrologic soil regimes in equilibrium numerical experiments with a climate model of intermediate complexity. Izvestiya, Atmos. Ocean. Phys. 44 (5), 279-287.
[4] Arzhanov, M., Eliseev, A., Demchenko, P., Mokhov, I., 2007. Modeling of changes in temperature and hydrological regimes of subsurface permafrost, using the climate data (reanalysis). Earth Cryosphere XI (4), 65-69.
[5] Saito K., Kimoto M., Zhang T., et al., 2007. Evaluating a High-Resolution Climate Model: Simulated Hydrothermal Regimes in Frozen Ground Regions and Their Change Under the Global Warming Scenario. J. Geophys. Res. 112 (F2), F02S11.
[6] Lawrence D. M. and A. G. Slater, 2005. A Projection of Severe Near-Surface Permafrost Degradation during the 21st Century. Geophys. Res. Lett. 32 (24), L24401.
[7] Oberman, N., 2008. Contemporary permafrost degradation of European North of Russia. In Proceedings of the Ninth International Conference on Permafrost, June 29 — July 3. Fairbanks, Alaska. 2. P. 1305-1310.
[8] Arzhanov, M.M., Demchenko, P.F., Eliseev, A.V., Mokhov, I.I., 2010. Modelling of subsidence of perennially frozen soil due to thaw for the Northern Hemisphere during the 21st century. Earth Cryosphere XIV (3), 37-42.

Estimations of hydrate stability in Baikal

S.N. Denisov
A.M. Obukhov Institute of Atmospheric Physics RAS, 3 Pyzhevsky, 119017 Moscow, Russia
denisov@ifaran.ru

Large volumes of methane are stored in subaqueous hydrate deposits. Because of projected warming, there is considerable concern that a water temperature increase will lead to dissociation of subaqueous hydrate deposits with release of potentially large amounts of methane [1]. Such a release could amplify atmospheric warming and possibly accelerate dissociation of remaining hydrates. This study assesses the stability of hydrates in Baikal.

Methane hydrates are stable at low temperature and high pressure. Water temperature in Baikal is about 3.5 °C on the depths higher than 200 m. Using the pressure-temperature equilibrium equation for hydrates [2], hydrate stability zone in Baikal sediments found to exist on the floor depths higher than 380 m. Total area extent of hydrate accumulations is about 23300 km^2. Assuming the geothermal gradient of 35 °C/km the thickness of hydrate stability zone in Baikal varies from 120 m on the 400 m floor depth to 520 m on 1600 m floor depth. It results in total of $1.68 \cdot 10^{11}$ $м^3$ of hydrates or about $2.3 \cdot 10^{13}$ $м^3$ of methane (~14 GtC) in assumption that hydrates occupy 5% of pore space in sediments [3].

Changes in hydrate stability zone for the Baikal floor depths of 400 m and 700 m are shown on fig.1. Current temperature profile in water and sediments (1) is shifted to new equilibrium state (2) after an 1 K increase in water temperature. Hydrate stability zone on the Baikal floor depths shallower than 400 m completely disappears. Its thickness reduces by 50 m on average and the area extent reduces by about 5%. It leads to release of about 1.2 GtC of methane which is comparable with about 0.5 GtC of total yearly methane emissions to atmosphere on Earth. But only small part of methane from subaqueous hydrates can reach the atmosphere and it may take thousands of years to achieve the equilibrium temperature in deep sediments.

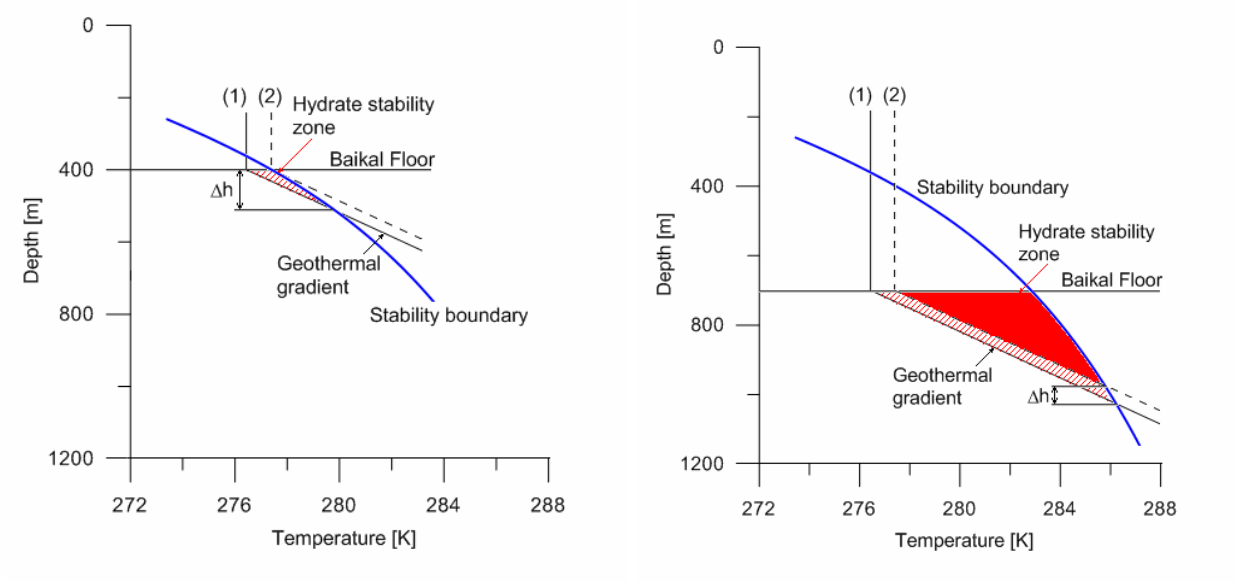

Fig.1 Changes of hydrate stability zone in Baikal due to 1K temperature increase for 400 m and 700 m floor depth.

Acknowledgments
NATO Collaborative Linkage Grant 983 725, Grant of the RF President Nsh-5467.2012.5, The Russian Foundation for Basic Research, The program of the Earth Sciences Department of the Russian Academy of Sciences, Programs of the Russian Ministry for Science and Education (contracts 403 14.740.11.1043, 16.525.11.5013, 21.519.11.5004, and 11.519.11.5006), Russian Academy of Science 74-OK/11-4.

References

[1] Denisov S.N., Arzhanov M.M., Eliseev A.V., Mokhov I.I. Assessment of the response of subaqueous methane hydrate deposits to possible climate change in the twenty-first century. *Doklady Earth Sciences. 2011. V. 441(2). P. 1706-1709.*

[2] Reagan M.T., Moridis G.J. Dynamic response of oceanic hydrate deposits to ocean temperature change. *J. Geophys. Res. 2008. V. 113. C12023.*

[3] Holbrook W.S., Hoskins H., Wood W.T., Stephen R.A., Lizaralde D. Methane Hydrate and Free Gas on the Blake Ridge from Vertical Seismic Profiling *Science. 1996. V. 273. P. 1840-1843.*

Mechanisms of negative cloud radiative feedback of stratocumulus and stratus in JMA-GSM SCM

Hideaki Kawai

Meteorological Research Institute, Japan Meteorological Agency

(e-mail: h-kawai@mri-jma.go.jp)

1. Introduction

In order to understand the mechanism of cloud radiative feedback of marine boundary layer clouds in climate models, a model intercomparison case CGILS (CFMIP-GCSS Intercomparison of Large-Eddy and Single-Column Models) was designed by Minghua Zhang. In the intercomparison case, three different regimes of marine low-level clouds are simulated: shallow cumulus (location: S6), stratocumulus (S11), and stratus (S12). The control climate forcing and the future climate forcing with sea surface temperature increased by 2 K are given for the simulation.

The Single Column Model (SCM) version of the operational global model of the JMA (Japan Meteorological Agency), GSM (Global Spectral Model), was used for the simulation. The results of two versions of this SCM are shown: one adopts an operational parameterization of stratocumulus (Sc) (Version 1, V1), and the other uses a test version of the Sc parameterization (Version 2, V2). The details of these versions are described by Kawai (2012) (see section 4 of this issue).

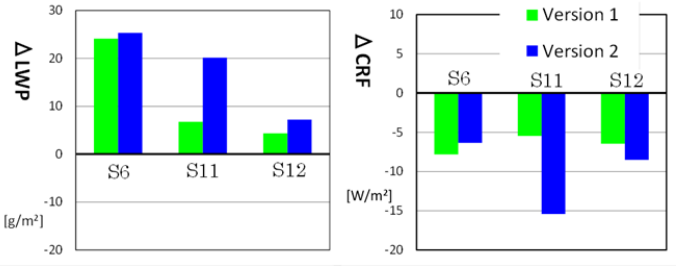

Fig. 1: Changes of liquid water path (left) and cloud radiative forcing (right) between the control climate and future climate forcing. Results are shown for S6, S11, and S12 using Sc scheme Version 1 and Version 2.

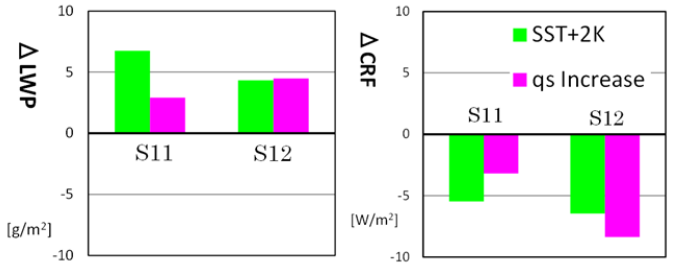

Fig. 2: Changes of liquid water path (left) and cloud radiative forcing (right) between the control climate and future climate forcing (light green), and between using the default parameterization and one with a modified calculation of in-cloud CWC. Results are shown for S11 and S12 using Sc scheme Version 1.

2. Negative cloud radiative feedback

The right-hand panel of Fig. 1 reveals that both versions of the JMA-GSM SCM show negative cloud radiative feedback for all cloud regimes (S6: shallow cumulus, S11: stratocumulus, and S12: stratus).

The left-hand panel shows that the liquid water path (LWP) increases for all cloud regimes, using either V1 or V2. The cloud cover is 100% for both the control and future climate forcing, at either S11 or S12, for either V1 or V2 (not shown). Therefore, the negative cloud radiative feedback is a consequence of the increase of LWP for S11 and S12. It is also worth mentioning that the magnitude of the change in cloud feedback is not proportional to the change of LWP: a larger change of LWP at S6 and a smaller change of LWP at S12 bring a comparable change in cloud radiative forcing (CRF). This is because LWP itself is larger at S6, and smaller at S12, and the relationship between LWP and albedo is nonlinear.

3. Mechanism of increase of LWP

To understand the mechanism of the increase of LWP due to the future climate forcing, simple numerical experiments are performed for each version of the Sc scheme, because the mechanisms could be different for the two parameterizations.

3.1. Mechanism in Sc scheme Version 1

In Sc scheme V1, in-cloud cloud water content (CWC) is determined by the following equation (Kawai 2012):

$$q_{c_{cld}} = \beta \cdot q_{sat}$$

As a simple test, the right-hand side of the equation is multiplied by 1.13 using the control climate forcing. This test is performed because when the temperature is increased by 2 K, the saturation specific humidity is increased by about 13%.

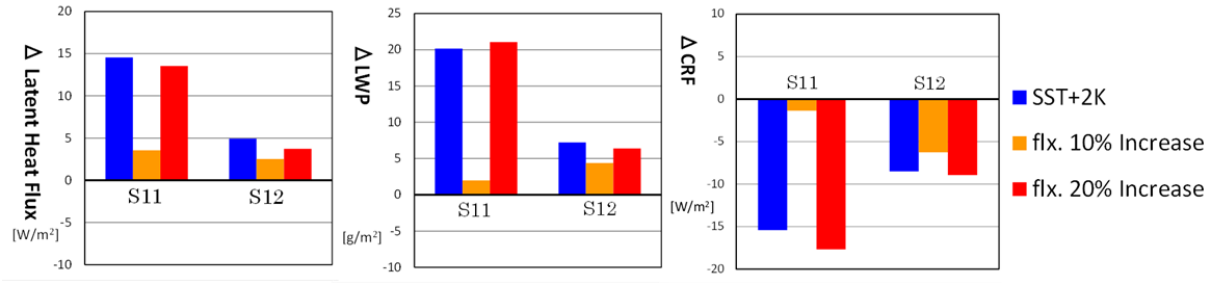

Fig. 3: Change of latent heat flux (left), liquid water path (middle) and cloud radiative forcing (right) between the control climate and future climate (blue), and between the default parameterization and that in which the calculated latent heat flux in the surface flux parameterization is increased by 10% (orange) or 20% (red). Results are for S11 and S12 using Sc scheme Version 2.

Fig. 2 shows that when the factor is increased in the simulation of control climate forcing, the changes of LWP and CRF are comparable to those with future climate forcing, although these changes are not quite identical quantitatively. This result implies that the increase of saturation specific humidity in the future climate contributes to the negative CRF feedback in this scheme. The same mechanism may also generate negative CRF feedback in those models where the same equation is used to determine in-cloud CWC (e.g., diagnostic cloud cover schemes based on relative humidity).

3.2. Mechanism in Sc scheme Version 2

In the case of Sc scheme V2, CWC is determined by a balance of many physical processes. However, the influence of the change of mixing at the cloud top can be ignored in this scheme because the mixing is set to zero (Kawai 2012). In this case, the balance "in the model" can be simplified as follows. There is positive feedback on CWC between radiative cooling at the cloud top and water vapor transport by turbulence. These two processes can create a balance with the conversion process of CWC to precipitation, because there is a negative feedback on CWC between the former two processes and the conversion process. Based on this concept, a simple test of increasing the latent heat flux is performed. For this purpose, when latent heat flux is calculated in the model by the following equation:

$$Q_E = \rho L C_h |U_1| (q_s - q_1),$$

the flux is multiplied by 1.1 or 1.2 for the control climate forcing simulation.

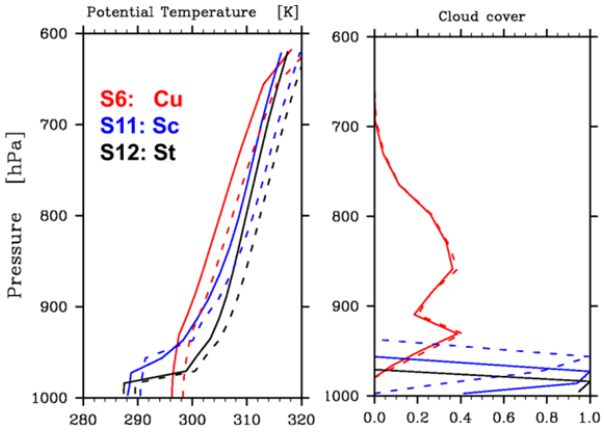

Fig. 4: Vertical profiles of potential temperature (left) and cloud cover (right) for S6, S11, and S12. Solid lines correspond to control climate forcing and dashed lines future climate forcing.

Figure 3 shows that when the latent heat flux is increased by 10%, the changes of latent heat flux, LWP and CRF are smaller than the changes with future climate forcing. However, it is also clear that those changes are comparable to the change with future climate forcing when the flux is increased by 20%. This result implies that the increase of latent heat flux in the future climate can be, at least partly, a cause of the increase of LWP and hence, negative cloud radiative feedback. It is worth noting that at S11, the changes are much larger for the case of a 20% increase in latent heat flux than for a 10% increase. This large change is caused by a change of vertical structure of the cloud layer. The cloud layer is lifted by one model vertical level at S11 with future climate forcing, as shown in Fig. 4. This discrete lift also occurs in the simulation with a 20% increase of latent heat flux, which destabilizes the sub-cloud boundary layer and results in a step-like transition in the balance among latent heat flux, LWP and CRF.

References

Kawai, H., 2012: Results of ASTEX and Composite model intercomparison cases using two versions of JMA-GSM SCM. *CAS/JSC WGNE Research Activities in Atmospheric and Oceanic Modelling/WMO*, **42**, section 4.

Climate change in Arctic and sea wave activity in the 21st century from model simulations

V.C. Khon, I.I. Mokhov, F.A. Pogarsky
A.M. Obukhov Institute of Atmospheric Physics RAS, Moscow, Russia
(khon@ifaran.ru)

Rapid climate change in the Arctic during the last decades is one of the most noticeable manifestations of global warming (Arctic Climate Impact Assessment; ACIA, 2005). Therefore, prognostic assessments of dangerous storm events and associated wave activity have very important implication for the potential planning the shelf exploration and marine navigation in Arctic basin, including the Northern Sea Route (Khon et al., 2010).

Two dimensional spectral numerical model for ocean surface waves (Polnikov, 2005) has been applied to analyze sea wave activity in Arctic basin using simulations with climate general circulation model CCSM3 (Collins et al., 2006) forced by SRES-A1B anthropogenic scenario for the 21st century. Figure 1 shows the histograms of the mean significant wave height distribution for five Russian Arctic seas. The horizontal axis represents ranges (according to Beaufort scale) of wave heights in meters for a developed wind waves on the high seas. The vertical axis is the percentage frequency (with respect to the total amount of events) of the different wave heights over the entire ice-free sea area for three decades: 1990-1999, 2040-2049 and 2090-2099.

For all analyzed seas except the Barents Sea, the model results show considerable increase in frequency of high waves (up to 2 m) in the 21st century with the strongest changes for the Laptev (~45% in the end of 21st century) and East-Siberian (more than 2 times in the middle of 21st century) Seas. This tendency is a result of the projected significant increase in ice-free water areas which is in favor of developing wave activity. For the Barents Sea model does not reveal significant changes in sea wave activity for the 21st century. For the frequency of very high (more than 5 meters) waves model simulations show a growth of activity in the middle and end of 21st century.

Similar analysis has been performed with WAVEWATCH III ocean surface waves model (Tolman, 2009) using simulations with the regional climate model HIRHAM (Rinke and Dethloff, 2008) forced by SRES-A1B anthropogenic scenario, in particular. There is a general agreement for sea wave activity estimates based on HIRHAM and CCSM3 climate simulations with remarkable differences for very high waves.

Despite very small frequency of extremely high sea waves (of the order of 1% for the Barents Sea, in particular) these waves are especially dangerous for shipping and offshore construction.

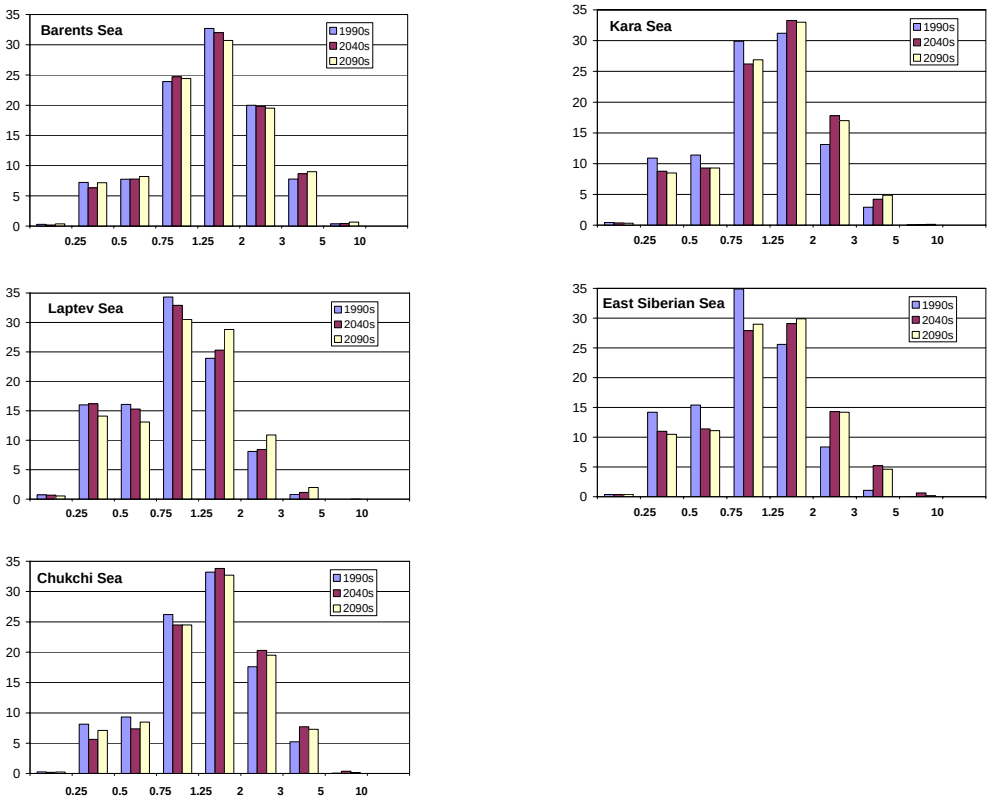

Figure 1. Histograms of the mean sea wave height (m) from model simulations for different Arctic Seas for three decades: 1990-1999, 2040-2049 and 2090-2099.

This work was supported by the Russian Foundation for Basic Research, the programs of Russian Academy of Sciences and Russian Ministry of Education and Science.

References

ACIA (2005) Arctic climate impact assessment. Cambridge University Press, Cambridge.

Collins W.D., Bitz C.M., Blackmon ML, Bonan G.B., Bretherton C.S., Carton J.A., Chang P., Doney S.C., Hack J.J., Henderson T.B. (2006) The community climate system model: CCSM3, *J Climate*, 19, 2122–2143

Khon V.C., Mokhov I.I., Latif M., Semenov V.A., Park W. (2010), Perspectives of Northern Sea Route and Northwest Passage in the twenty first century, *Climatic Change*, 100, 757–768, doi:10.1007/s10584-009-9683-2.

Polnikov V.G. (2005) Wind-wave model with an optimized source function, *Izvestiya, Atmospheric and Oceanic Physics*, 41(5), 594-610.

Rinke A, Dethloff K (2008) Simulated circum-Arctic climate changes by the end of the 21st century, *Global and Planetary Change*, 62, 173–186.

Tolman H.L. (2009) User manual and system documentation of WAVEWATCH III version 3.14. NOAA/NWS/NCEP/MMAB Technical Note 276 (*http://polar.ncep.noaa.gov/mmab/papers/tn276/MMAB_276.pdf*)

Analysis of CMIP5 historical runs for south west US precipitation

S. Langford and D. Noone
Department of Atmospheric and Oceanic Science, and
Cooperative Institute for Research in Environmental Sciences
University of Colorado, Boulder, CO, USA
sally.langford@colorado.edu

We examined historical runs from the CMIP5 archive to evaluate model performance against present climate. We focus on mechanisms linked to decadal variations in south west US precipitation, and the occurrence of drought. Drought is characterized by a prolonged lack of moisture, due to anomalous subsidence, diverted storm tracks, or low soil moisture. Our analysis indicates that variability in precipitation in the south west US in summer and winter, which may result in periods of drought, is associated with specific atmospheric circulation patterns arising from sea surface temperature anomalies in the Pacific Ocean. The Great Basin region (32-42^{o}N, 242-254^{o}E; Meehl and Hu 2006) is used to characterize the hydrological climate of the south west US, and 130 years of NOAA-CIRES 20th century reanalysis data is compared to the CMIP5 model historical runs.

The winter (DJF) precipitation in the south west US is dominated by storms arriving across the coast of California. In the observations, this precipitation extends east to the Rocky Mountains at around 108^{o}W. Precipitation on the east side of the mountains is predominately due to the summertime (JJA) North American monsoon (Douglas et al. 1993). In the models, the cutoff between the summer and winter precipitation regimes is shifted west to around 110^{o}W, due in part to errors in representing the effects of topology and varying model resolutions. Figures 1 and 2 show the standardized anomalies of area averaged precipitation regressed onto geopotential height or SST anomalies for five-year averages of a single season. In winter, higher than average precipitation in the south east US is associated with coastal low pressure and high height anomalies over northern North America (Fig 1a, 2a). Warm equatorial Pacific Ocean and local SST anomalies are related to the magnitude of the winter precipitation anomaly (Fig 1d, 2d). The average of the CMIP5 model results is consistent with the observations, due to their ability to accurately represent coastal storms. Cool northern Pacific SST anomalies are correlated with precipitation in the north-west of the continent near Vancouver. This influence can extend as far south as the Great Basin region, however it is not the main source of variability in the south west US in this season.

In summer, higher than average precipitation in the Great Basin region is associated with anomalously high heights over North America, and lower than average heights over the north east Pacific Ocean (Fig 1b, 2b). This relationship, which is highly correlated with monsoon precipitation in Mexico, Arizona and New Mexico, is weaker for the average of the models than for the observations. Precipitation from the north east of the Great Basin region, separate to the monsoon signal, is associated with high height anomalies over Canada, and low height anomalies over the US (Fig 1c, 2c). While the observations show that this precipitation anomaly is associated with positive SST anomalies in the northern Pacific Ocean (Fig 1f), the models show the opposite response (Fig 2f), suggesting that even the sign of the atmospheric bridge is not robust in the models. Likewise, warmer than usual ocean surface temperatures near the Gulf of California (Fig 1e) are correlated with higher than usual monsoon precipitation in the observations only. This may be due to variation in the spatial extent of monsoon precipitation in the models, associated with errors in the location of the monsoon ridge, and the failure to accurately capture the reversal of winds due to surface heating. Therefore, the atmospheric bridge between SST anomalies and south west US precipitation anomalies on decadal timescales is not well represented by the CMIP5 historical runs in summer.

There is evidence of an atmospheric bridge between typical SST anomalies in the north Pacific Ocean and near the Gulf of California to south west US precipitation in reanalysis data in summer and winter. This may be useful in predicting decadal drought in the Great Basin region if the SST anomalies are predictable on long time scales. However, the CMIP5 model historical runs are unable to robustly match the observational results for summer, despite some indication of similar circulation patterns.

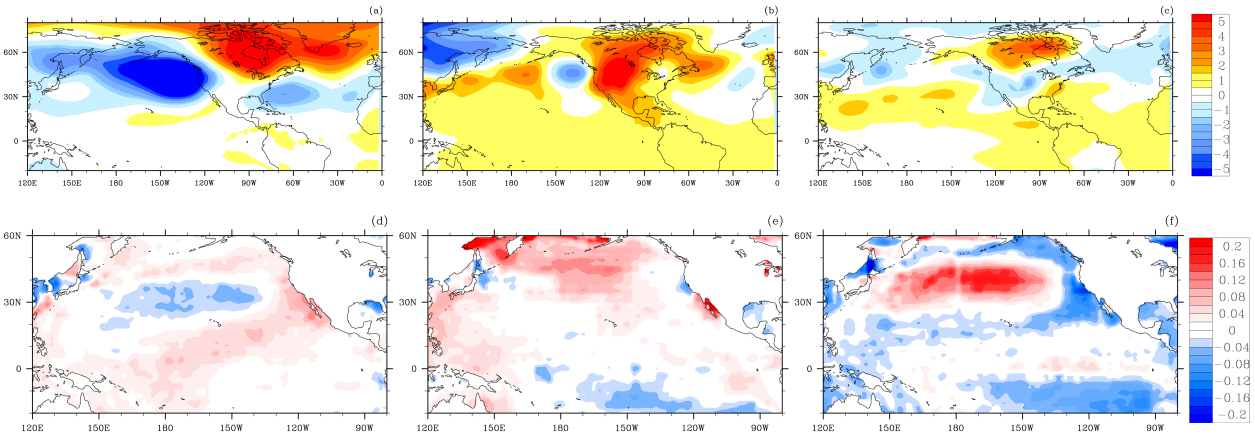

Fig 1. Results for observational data. (a)-(c) Precipitation standardized anomalies regressed onto 500hPa geopotential height anomalies (a) for west SW US precipitation in DJF, (b) for SW US precipitation in JJA, (c) for east SW US precipitation in JJA. Units are the geopotential height anomaly in meters associated with one standard deviation increase in precipitation. (d)-(f) Precipitation standardized anomalies regressed onto SST anomalies (a) for west SW US precipitation in DJF, (b) for SW US precipitation in JJA, (c) for east SW US precipitation in JJA. Units are the SST anomaly in Kelvin associated with one standard deviation increase in precipitation.

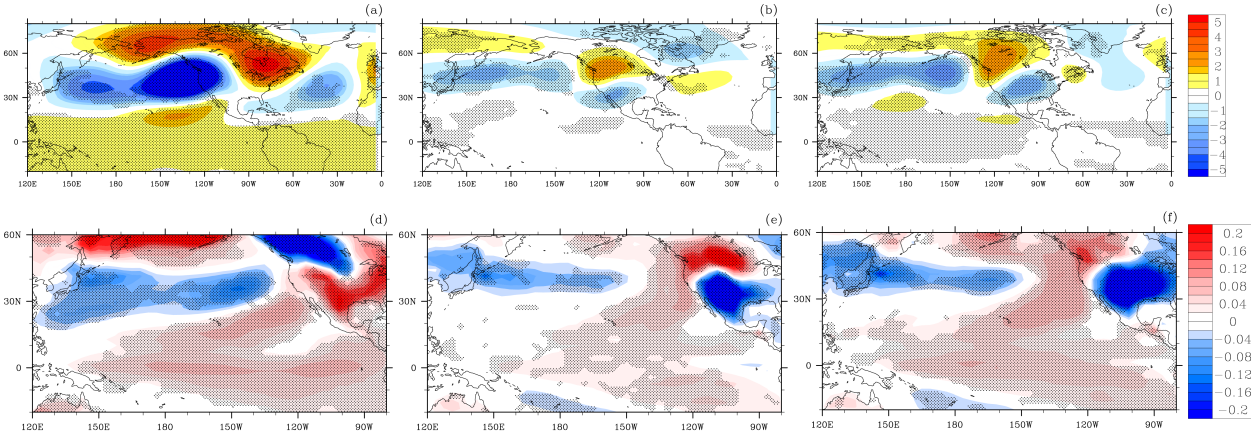

Fig 2. As above, for average of CMIP5 models re-gridded to a common resolution. (d)-(f) Precipitation index is regressed onto skin temperature, which is the SST over oceanic regions. Hatching indicates that two-thirds of the models agree on the sign of the result.

Acknowledgement

This research is part of the Investigation of Decadal Climate Predictability and Hydroclimate Impacts (IDCPI) on the Western US project, which is supported by the National Science Foundation, Division of Atmospheric and Geospace Sciences, Paleoclimate. We acknowledge the World Climate Research Programme's Working Group on Coupled Modelling, which is responsible for CMIP, and we thank the climate modeling groups for producing and making available their model output. For CMIP the U.S. Department of Energy's Program for Climate Model Diagnosis and Intercomparison provides coordinating support and led development of software infrastructure in partnership with the Global Organization for Earth System Science Portals. 20th Century Reanalysis V2 data provided by the NOAA/OAR/ESRL PSD, Boulder, Colorado, USA, from their Web site at http://www.esrl.noaa.gov/psd/.

References

Douglas, M.W., R.A. Maddox, K. Howard and S. Reyes, 1993: The Mexican Monsoon. *J. Clim.*, **6**, 1633-1677

Meehl, G.A., and A. Hu, 2006: Megadroughts in the Indian Monsoon Region and Southwest North America and a Mechanism for Associated Multidecadal Pacific Sea Surface Temperature Anomalies. *J. Clim.*, **19**, 1605-1623.

Summer Blockings in Euro-Atlantic Region from Model Simulations

I.I. Mokhov, M.G. Akperov and A.A. Timazhev

A.M. Obukhov Institute of Atmospheric Physics RAS, Moscow, Russia
mokhov@ifaran.ru

The Russian heat wave in summer 2010 was associated with an anomalous blocking situation (with total duration about two months) over the European part of Russia. Frequency of atmospheric blockings in the Euro-Atlantic region in summer season has a maximum near 30°E over Eastern Europe (Wiedenmann et al., 2002). Estimates based on observations and model simulations (Lupo et al., 1997; Mokhov and Petukhov, 1997) display a tendency of increase of blockings duration under general warming.

Similar to (Mokhov et al., 2011) we analyzed possible changes of atmospheric blockings activity in the Northern Hemisphere (NH) from different climate model simulations for the 21st century with various scenarios. In particular, the CMIP3 simulations with global climate models (GCMs) were used. Special attention was paid to the analysis of summer blockings in the Euro-Atlantic region (60°W-60°E) with an assessment of risk and potential predictability for extreme total duration of blockings.

According to results of analysis of simulations the most comprehensive global climate models have an ability to reproduce extreme blocking situations in the atmosphere. At the same time results are sensitive to the choise of criteria for blockings as well to the scenarios (initial conditions) used.

Figure 1 shows an example of interannual variations for total blockings duration over Euro-Atlantic region (60°W-60°E) in summer from the IPSL-CM4 GCM simulations for 1960-2100 with anthropogenic scenarios SRES-A1B and SRES-A2 for the 21st century and with various criteria for blockings (see also (Mokhov et al., 2009)). In particular, modified Lejenas-Okland criteria were used similar to (Wiedenmann et al., 2002) with stronger (version I) or weaker (version II) conditions for longitudinal size of blockings.

Analysis of possible changes in the extratropical cyclonic and anticyclonic activity displays large variability in the 21st century from different model simulations with anthropogenic forcing (Mokhov et al., 2009). Blocking anticyclones also display remarkable interannual and interdecadal variability.

It can be expected according to Fig. 1 an extreme total duration of blocking situation in summer for the NH Euro-Atlantic region up to about 60 days and even longer. The anomalous total duration of blocking situation about 60 days in Euro-Atlantic region was obtained for summer 2010 in the considered model simulations with the SRES-A1B scenario and with one of applied criteria for blockings (I). This model estimate is close to real duration of blocking situation for European part of Russia in summer 2010. Model simulations show possibility of other summer blockings in the Euro-Atlantic region with duration about two months in the 21st century, in particular in 2020 and 2022 for the SRES-A1B scenario or in 2043 and 2081 for the SRES-A2 scenario. The largest total duration of summer blockings over the Euro-Atlantic region before 2010 was detected from model simulations (since 1960) in 1973.

With a weaker conditions for longitudinal size of blockings (II) the total duration of blocking situation was detected even longer (about 10 weeks) for Euro-Atlantic region in summer 2010.

Blockings characteristics display nonlinear changes in dependence on climate changes.

This work was supported by RFBR, RPSG, RAS and MESRF.

References

Lupo A.R., R.J. Oglesby and I.I. Mokhov, 1997: Climatological features of blocking anticyclones: A study of Northern Hemisphere CCM1 model blocking events in present-day and double CO_2 concentration atmospheres. *Climate Dyn.*, **13**, 181–195.

Mokhov I.I., 2011: Specific features of the 2010 summer heat formation in the European territory of Russia in the context of general climate changes and climate anomalies. *Izvestiya, Atmos. Oceanic Phys*., **47**(6), 653-660.

Mokhov I.I., M.G. Akperov, J.-L. Dufresne and H. Le Treut, 2009: Cyclonic activity and its total action over extratropical latitudes in Northern Hemisphere from model simulations. *Research Activities in Atmospheric and Oceanic Modelling*, J. Cote (ed.), Rep.39(7), 9-10.

Mokhov I.I., M.G. Akperov and A.A. Vetrova, 2011: Russian heat wave and blockings activity changes. *Research Activities in Atmospheric and Oceanic Modelling*, A. Zadra (ed.), Rep.41(7), 13-14.

Mokhov I.I. and V.K. Petukhov, 1997: Blockings and their tendencies of change. *Doklady Earth Sci*., **357**, 687-689.

Wiedenmann J.M., A.R. Lupo, I.I. Mokhov and E.A. Tikhonova, 2002: The climatology of blocking anticyclones for the Northern and Southern Hemispheres: Block intensity as a diagnostic. *J. Climate*, **15**(23), 3459–3473.

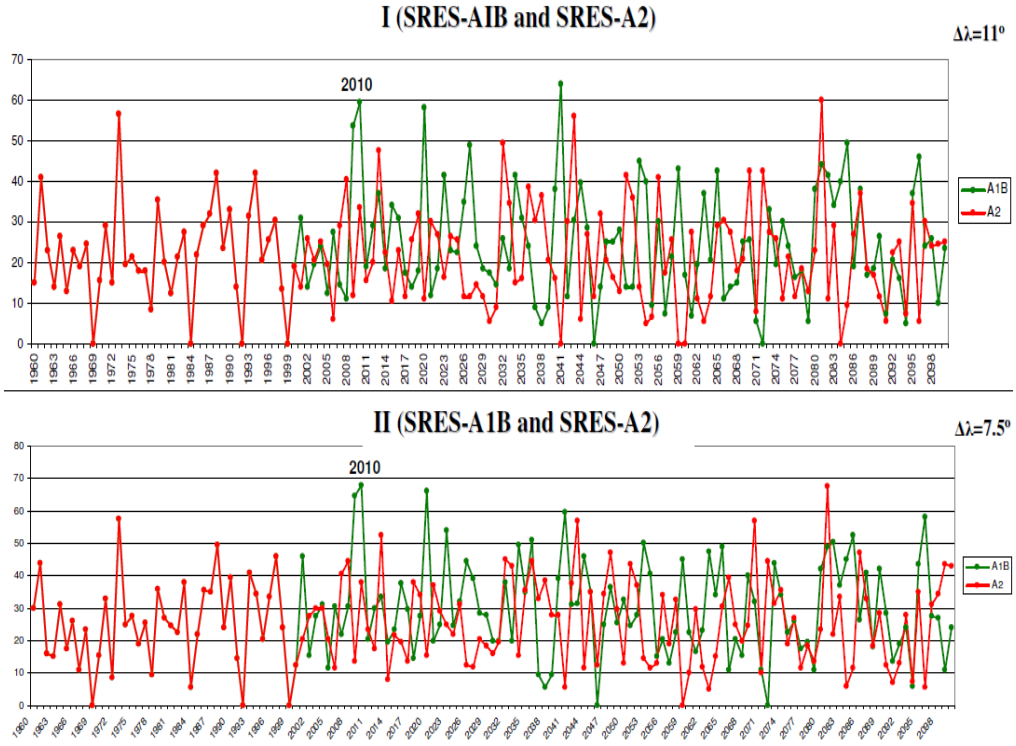

Figure 1. Interannual variations of total blockings duration over Euro-Atlantic region (60°W-60°E) in summer from model simulations with different SRES (A1B and A2) scenarios and with various criteria for blockings (I and II).

Oceanic carbon uptake in the simulation with the IAP RAS global climate model.

K.E. Muryshev[1], A.V. Eliseev[1], V.A. Gorchakov[2], V.A. Ryabchenko[2], and I.I. Mokhov[1]

[1] A.M. Obukhov Institute of Atmospheric Physics RAS,
3 Pyzhevsky, 119017 Moscow, Russia, e-mail: kmuryshev@mail.ru

[2] P.P. Shirshov Institute of Oceanology RAS, St.-Petersburg Branch,
30, 1 Liniya, Vasilievskiy Ostrov, 199053 St.-Petersburg, Russia

The climate model of intermediate complexity developed at the A.M. Obukhov Institute of Atmospheric Physics RAS (IAP RAS CM) [1] is extended by the state-of-the-art oceanic carbon cycle module [2]. The IAP RAS CM's carbon cycle is closed by respective terrestrial module and the atmospheric CO_2 compartment in a well-mixed approximation [3, 4]. A simulation with the IAP RAS CM is performed which is forced by fossil fuel+industrial CO_2 emissions, by atmospheric concentrations of CH_4, N_2O, tropospheric and stratospheric sulphates, by changes in extent of crops and pastures and by variations in total solar irradiance. These agents were prescribed according to protocol "Historical simulation" for 1765-2005 and according to scenario RCP 2.6 in 2006-2100 (for more details, see http://cmip-pcmdi.llnl.gov/cmip5/forcing.html).

In these simulations, the IAP RAS CM realistically reproduces basic characteristics of the global carbon cycle. In particular, the 20th century deviations of the simulated carbon dioxide content from the observed one are not larger than 7 ppmv. Global oceanic carbon uptake $F_{CO2,o}$ in 1980s (1990s) in the model is 1.5 PgC/yr (1.9 PgC/yr) which is within the respective uncertainty range 1.8±0.8 PgC/yr (2.2±0.4 PgC/yr) [5], see Fig. 1. Its spatial distribution is in reasonable agreement with the empirical data [6] (Fig. 2, top panel). Under the RCP 2.6 scenario, $F_{CO2,o}$ continues to increase till the middle of the 21st century reaching 4.1 PgC/yr and decreases thereafter amounting 3.3 PgC/yr in year 2100. Most marked changes are predicted in high latitudes due to receding sea ice which exposes more open ocean water to atmosphere (Fig. 2, bottom panel).

This work has been supported by the the President of Russia grant 5467.2012.5, by the Russian Foundation for Basic Research, and by the Programs of the Russian Ministry for Education and Science (contracts 14.740.11.1043, 21.519.11.5004, 11.519.11.5006, and 74-OK/11-4), and the Russian Academy of Sciences.

References:

1. Muryshev, K.E., A.V. Eliseev, I.I. Mokhov, and N.A. Diansky, 2009: Validating and assessing the sensitivity of the climate model with an ocean general circulation model developed at the Institute of Atmospheric Physics, Russian Academy of Sciences. Izvestiya, Atmos. Ocean. Phys., 45 (4), 416-433, doi: 10.1134/S0001433809040033.

2. Popova, E.E., V.A. Ryabchenko, and M.J.R. Fasham, 2000: Biological pump and vertical mixing in the Southern Ocean: Their impact on atmospheric CO_2. Glob. Biogeochem. Cycles, 14 (1), 477-498, doi: 10.1029/1999GB900090.

3. Eliseev, A.V., 2011: Estimation of changes in characteristics of the climate and carbon cycle in the 21st century accounting for the uncertainty of terrestrial biota parameter values. Izvestiya, Atmos. Ocean. Phys., 47 (2), 131-153, doi: 10.1134/S0001433811020046.

4. Eliseev, A.V., and I.I. Mokhov, 2011: Uncertainty of climate response to natural and anthropogenic forcings due to different land use scenarios. Adv. Atmos. Sci., 28 (5), 1215-1232, doi: 10.1007/s00376-010-0054-8.

5. Solomon, S., et al., Eds., 2007: Climate Change 2007: The Physical Science Basis. Cambridge University Press, Cam-bridge/New York.

6. Takahashi T., et al., 2009: Climatological mean and decadal change in surface ocean pCO2, and net sea-air CO_2 flux over the global oceans . Deep-Sea Res. II, 56 (8-10), 554-577, doi: 10.1016/j.dsr2.2008.12.009.

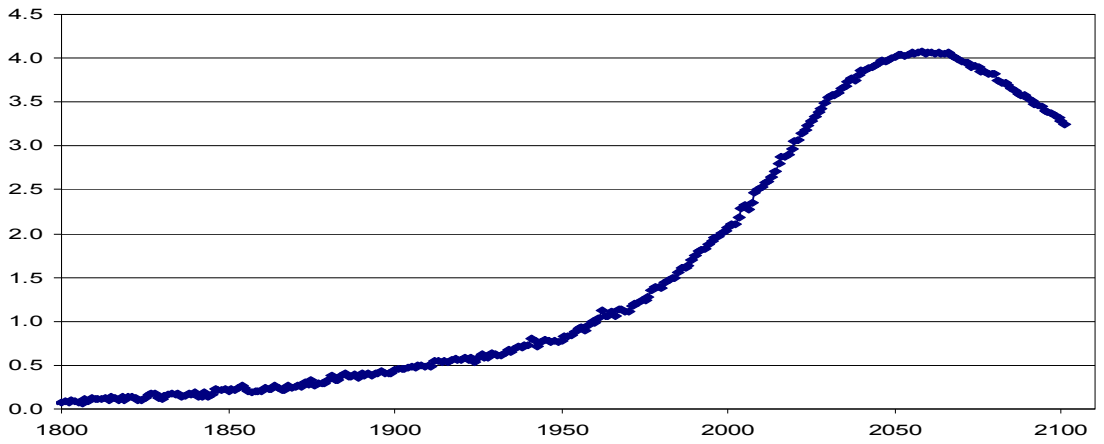

Fig. 1. Global oceanic CO_2 uptake [PgC/yr] vs. time.

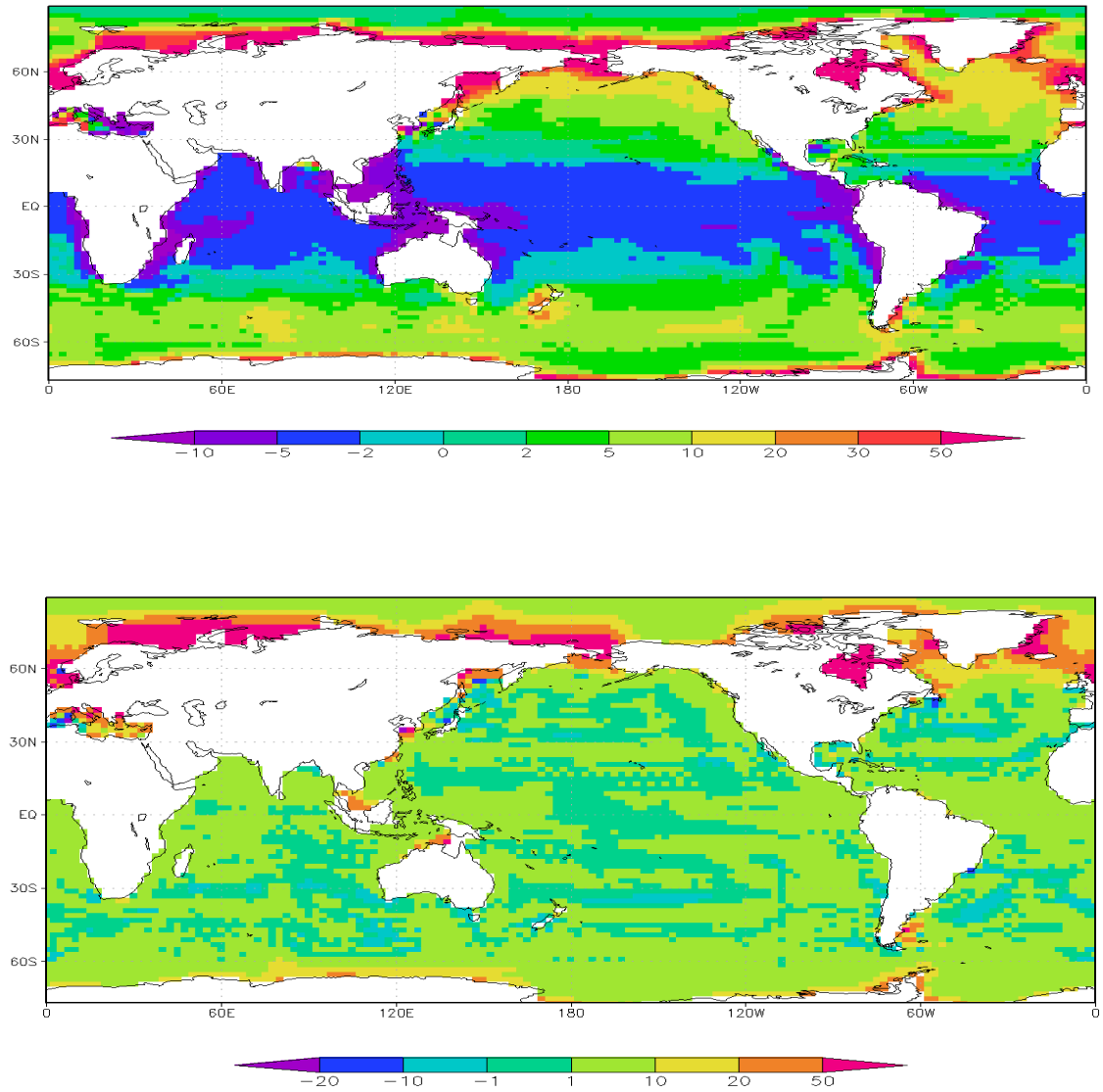

Fig. 2. Oceanic carbon uptake per unit area [grams C m^{-2} yr^{-1}] averaged for 1991-2000 (top) and change of this uptake from 1991-2000 to 2091-2100 (bottom).

GLOBAL AND INDOCHINA CLIMATE MODELLING

V.P. Parkhomenko
Computing Centre of the Russia Academy of Sciences
Vavilov Str. 40 Moscow 119967 Russian Federation
E-mail: parhom@ccas.ru

Numerical experiments with the coupled climate models of general circulation will be carried out. It is supposed to perform statistical analysis of physical fields, derived from simulation. Comparing of these results with observational data and model calculations on various models is to be done. Investigation of the climate warming influence on the Pacific thermohaline circulation and regional climate in Indochina is to be performed. Investigation of the Pacific Ocean pollution influence on the climate and biosphere processes at Indochina and South China Sea is planning. We will obtain forecasts of global and regional dynamics of environmental and agricultural processes based on mathematical models of biogeochemical cycles and crop yields. It is expected to get predictions of global warming, based on different scenarios of anthropogenic-technogenic activity, including the limitations of the Kyoto Protocol and the post-Kyoto agreements, the various options of limited implementation of agreements, especially with the growth of energy production and carbon dioxide emissions increase in the countries of Indochina. Research is to be conducted on Indochina data, and especially on the developing Vietnam.

It is suggested to realize the next research plan agreed with foreign partners:

- Development of a coupled global model of the thermohaline ocean circulation and atmospheric general circulation model.
- Collecting and preparing data for numerical simulations to reproduce the climate sensitivity with Global climate model.
- Planning for the computational experiments, the research models to produce forecasts of the global dynamics processes, including global warming, based on different scenarios of anthropogenic- technogenic activity, including the Kyoto Protocol and the various options for its not full implementation, and the implementation of new post-Kyoto scenarios.
- Preparation of the biosphere and climate stability estimates based on the Kyoto Protocol scenarios.
- Investigation of the climate warming influence on the Pacific thermohaline circulation and the regional European climate.
- Investigation of the influence of ocean pollution on climate and biosphere processes.
- Development and implementation of joint models of climate and biogeochemical cycles for the interactive processes of CO2 transport and exchange of ocean - atmosphere - terrestrial ecosystems.

During the project execution will be developed and implemented the new versions of the global climate models. Model ocean block is based on the spatial thermohaline (describing the circulation caused by the distribution of temperature and salinity) equations, with the addition in the horizontal momentum equations the linear friction term [1]. Temperature and salinity satisfy individual advection-diffusion equations. Procedure also takes into account the convective adjustment.

To describe the processes in the atmosphere is supposed to use one of the two models. The first is the atmospheric general circulation model [2]. The second is two-dimensional energy and humidity model. Prognostic variables in it are the atmosphere temperature and

specific humidity near the land surface. Dynamic equations in the model of sea ice are solved for its capacity and for the average ice thickness. This formulation of the problem will lead to possibility to carry out calculations about the time thousands of years, taking into account the evolution of deep ocean [3].

The climate warming influence on Pacific thermohaline circulation and Indochina regional climate, the impact of pollution on ocean climate and biosphere processes will be studied in models. Developed models are also expected to use for the ensemble of calculations for optimizing the parameters of the model and study the dependence of the results of the initial data [4]. It will be developed the atmosphere carbon dioxide transport model, using climate model results and the spatial model of the production process of terrestrial ecosystems in the seasonal regime.

It is supposed to conduct computational experiments, to obtain forecasts of the global dynamics processes, including global warming, based on different scenarios of anthropogenic-technogenic activity in Indochina and South China Sea, including the Kyoto Protocol and the various options for the lack of full implementation, execution new post-Kyoto scenarios. It is supposed to obtain estimates of the stability of the biosphere and climate scenarios based on the Kyoto Protocol [5].

References

1. V.P. Parkhomenko Seasonal Climate Model with Thermohaline Circulation Description. Research activities in atmospheric and oceanic modeling. World Meteorological Organization Geneva Switzerland 2009, V. 39, p. 7-11.
2. Пархоменко В.П. Проблемы изменения и моделирования климата. Сборник трудов. II Всероссийская научная конференция "Математическое моделирование развивающейся экономики" ЭКОМОД-2007, г. Киров, 9-15 июля 2007 г. И: Вятский государственный университет. С. 174-185.
3. Пархоменко В. П. Численные эксперименты с использованием глобальной климатической модели. Сообщения по прикладной математике. М.: ВЦ РАН, 2010. 36 с.
4. К.П. Беляев, Г.М. Михайлов, В.П. Пархоменко, В.А. Соколов, Н.П. Тучкова Численное моделирование климатических процессов с применением методики ансамблевых экспериментов. М: ВЦ РАН, 2010. ISBN 978-5-91601-038-1, 132 с.
5. Tarko A.M. (2005). Anthropogenic Changes of the Global Biosphere Processes. Mathematical Modeling. - Moscow. Fizmatlit. 2005. 232 pp. (in Russian).